Hindawi
Geofluids
Volume 2021, Article ID 6634673, 19 pages
https://doi.org/10.1155/2021/6634673

Research Article

Stability Analysis of Underground Pillar Supporting System under Different Disturbed Stresses

Yang Li,[1] Limin Liu,[2] Jinpeng Zhang,[3] Chuanxiao Liu,[3] Mengyao Zhang,[2] and Xiujuan Wang[2]

[1]*College of Safety and Environmental Engineering, Shandong University of Science and Technology, Qingdao 266590, China*
[2]*College of Energy and Mining Engineering, Shandong University of Science and Technology, Qingdao 266590, China*
[3]*College of Water Conservancy and Civil Engineering, Shandong Agricultural University, Tai'an, Shandong 271018, China*

Correspondence should be addressed to Limin Liu; llmsdust@163.com and Jinpeng Zhang; zjpsdust@126.com

Received 11 December 2020; Accepted 31 May 2021; Published 22 June 2021

Academic Editor: Chun Zhu

Small external disturbances may destabilize the bearing pillar, which in turn will change the stress distribution of the pillar supporting system, leading to its overall instability. Based on the engineering background of a mine and the mechanical analysis of pillar under disturbed stress, this paper investigated the stress, strain, and plastic zone of the pillar supporting system under different disturbed stresses. Then, the chain instability of the pillar supporting system was achieved. The law of stress transfer and plastic development of the pillar supporting system was explored. The results showed that the greater the disturbed stress, the faster the increase rate of the maximum stress of the pillar supporting system. As the width of the pillar increased, the maximum stress of the pillar decreased, so its risk of damage decreased. As the disturbed stress increased, the maximum principal strain and equivalent plastic strain of the 6 m wide pillar increased approximately linearly, and their growth rates of the 4 m wide pillar gradually increased. In the process of chain instability of the pillar supporting system, the sides of the middle pillar were destroyed first, and then the plastic zone gradually penetrated, causing the stress of the adjacent pillar to increase, which in turn led to its destruction. By analyzing the monitoring data of stress, displacement, or plastic strain, the instability of the pillar can be predicted.

1. Introduction

As the number of underground mines increases, so does the number of mined-out areas [1–3]. The stability of the goaf directly affects the structure of the overlying strata [4–6]. After the goaf is unstable, the overlying strata gradually bends, sinks, and collapses and finally extends to the surface [7–10]. So, the stability of the goaf directly affects the surface buildings and the ecological environment, as shown in Figure 1 (12.25 collapse accident of Pingyi gypsum mine). At present, the overlying strata are supported by pillars to prevent the instability of the goaf and surface collapse [11–13]. So, the stability of the goaf is mainly determined by the pillar and the roof strata. Many scholars have studied the stability of the goaf through the elastoplastic theory [14], catastrophe theory [15, 16], rheological theory [17, 18], fuzzy theory [19], and limit equilibrium theory [3, 20].

A support system consists of multiple pillars and roof-floor strata. The pillar supporting system is in a balanced state when it is stable. However, many factors may cause stress redistribution in the pillar supporting system, which in turn may cause instantaneous goaf instability [21–23]. There are main self-factors and external factors that affect the stability of the pillar. The self-factors include the mechanical properties, internal cracks, size, and structural characteristics of pillars [24–28]. The external factors include burial depth, in situ stress, treatment method of goaf, overburden stratum structure, water environment, and dip angle. For example, Ghasemi et al. [29] put forward an intelligent approach to predict pillar sizing in designing room-and-pillar coal mines. Cording et al. [30] investigated the effect of width-height ratio, stress slabbing, and slaking on pillar capacity. Wagner et al. [31] evaluated the effects of panel dimensions on loads in pillar systems. Yu et al. [32] investigated

Figure 1: 12.25 collapse accident of Pingyi gypsum mine.

the stress and deformation of longwall coal pillars located in a weak ground. Chen et al. [33] investigated the effects of original macrocracks in coal on the rockburst tendency.

The pillar supporting system is a complex dynamic system. Any change may cause the stress redistribution of the pillar supporting system or even its failure [8]. So, it is necessary to study the law of stress and strain distribution of the pillar supporting system. The destruction of local pillars in the system may cause the overall instability of the goaf. Under the static and dynamic load of the overlying strata, the stress concentration occurs locally in the pillar, which may reach its maximum bearing capacity. The destabilized pillar has little ability to support the roof rock. The load of the roof strata layer is transmitted to the adjacent pillar. So the adjacent pillar may be destroyed, which in turn may cause the overall instability of the pillar supporting system. So, the instability of a single pillar may cause the overall instability of the pillar supporting system. This phenomenon is similar to the domino effect, so it is called the domino instability effect of the pillar supporting system.

Therefore, this paper took the pillar supporting system under the engineering background as the research object. Based on the mechanical analysis of pillar under disturbed stress, the finite element software was used to study the stress distribution of the pillar supporting system under the initial in situ stress conditions. Then, the distribution rules of the stress, strain, and plastic zone of the pillar supporting system with 4 m and 6 m wide pillars under different disturbed stresses were investigated. Finally, the chain instability of the pillar supporting system was achieved by reducing pillar wide. In the process of instability, the stress transfer and plastic development of the pillar supporting system were explored.

2. Mechanical Model of Pillar under Disturbed Stress

According to the static-dynamic load model of a single pillar established by Li et al. [34], its force was analyzed, as shown in Figure 2. The deformation modulus and Poisson's ratio of the pillar are E and μ, respectively. Under the influence of the overburden, the pressure on the upper boundary of the pillar was P. The change of disturbed stress with time t was $P(t)$.

According to Newton's Second Law, the force motion equation of the pillar under static-dynamic coupling loading is

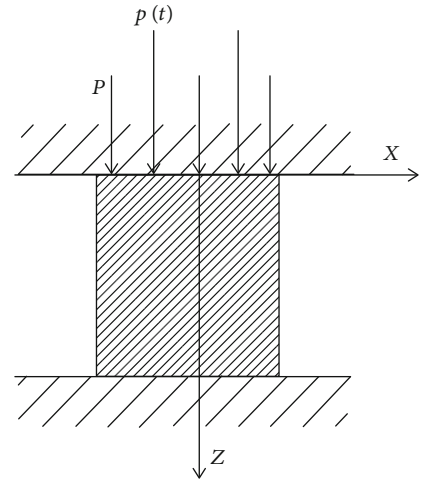

Figure 2: Static-dynamic load model of a single pillar.

$$ma + R(z) = P + P(t), \tag{1}$$

where m is the mass of the pillar, a is the acceleration of the pillar under disturbed stress, and $R(z)$ is the ability of the pillar to resist damage.

The disturbed stress propagates in the pillar as a wave. The deformation of the pillar is mainly in the z direction, so this article only analyzes the stress and deformation in the z direction. Assuming that the pillar is still in an elastic state under static and dynamic loads, the axial stress, strain, and movement speed of the pillar are as follows:

$$\begin{cases} \xi_z = \xi_0 + \dfrac{\partial f(z-ct)}{\partial z}, \\ \sigma_z = \sigma_0 + \dfrac{E(1-\mu)}{(1+\mu)(1-2\mu)} \cdot \dfrac{\partial f(z-ct)}{\partial z}, \\ v = -c \cdot \dfrac{\partial f(z-ct)}{\partial z}, \end{cases} \tag{2}$$

where ξ_z is the axial strain of the pillar, σ_z is the axial stress of the pillar, v is the axial movement speed of the pillar, σ_0 is the initial stress of the pillar under static load, ξ_0 is the initial axial strain of the pillar under static load, and c is the propagation speed of the wave in the pillar.

It can be seen that the strain and stress of the pillar are closely related to the disturbed stress. The force

Table 1: The mechanical parameters of the pillar supporting system in the numerical model.

Density (kg·m^{-3})	Elastic modulus (MPa)	Poisson's ratio	Cohesion (MPa)	Internal friction angle (°)	Compressive strength (MPa)
1471	2763.86	0.2521	1.34	25	14.80

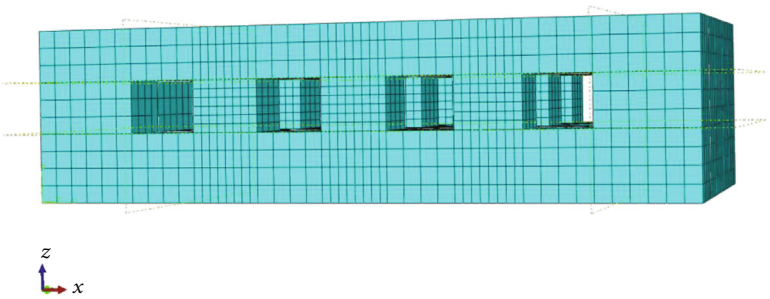

Figure 3: Model division of pillar supporting system.

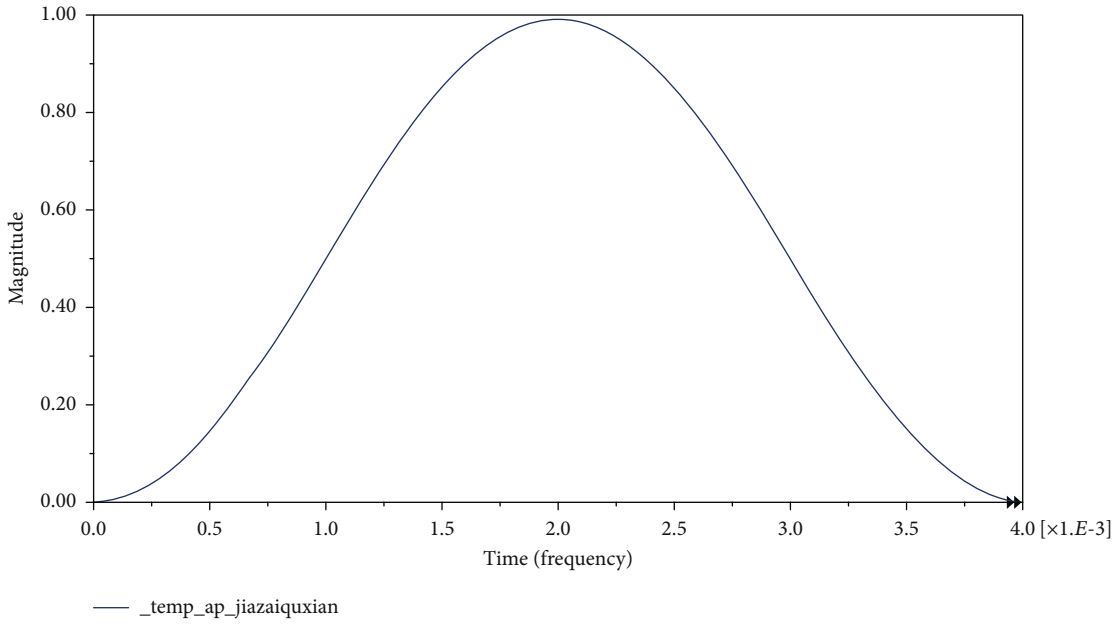

Figure 4: Perturbation curve of stress wave.

characteristics of the pillar is the key to determining whether it is damaged. Under the static and dynamic loads, the surface cracks of the pillars will develop internally, leading to the continuous expansion of plastic zone. The disturbed stress increases the elastic strain energy inside the pillar, making it more prone to dynamic disasters during the mining process. So, this is a threat to the stability of the pillar supporting system. Therefore, the influence of disturbed stress on the stability of pillar supporting system was investigated below.

3. Numerical Model and Scheme

For coal seams under villages, roads, and buildings, the strip mining methods are the most widely used. The width of the pillars in deep mines is often very large. Through numerical simulation, it is extremely difficult to investigate the failure rule of the wider pillars. So, the room-and-pillar mining scheme of the shallow coal seam in a mine was selected. The stability of the pillar supporting system under static and dynamic loads was studied by numerical simulation. The destruction of the pillars complied with the Mohr-Coulomb criterion.

3.1. Numerical Model. According to a coal mine, the numerical model of the pillar supporting system was established. According to the data provided by the coal mine, we know the basic parameters of coal and rock formations. The buried depth of the pillar is about -165 m. The average bulk density of the overlying rock layer is 2.0 kN/m^3. The self-weight stress of the overlying rock layer on the pillar is 3.3 MPa. The thickness of the coal seam is 4 m. The height and thickness of the pillars are both 4 m. The pillar width is 4 m. In order to investigate the failure rule of the pillars with different sizes under disturbed stress, the pillar widths were selected to

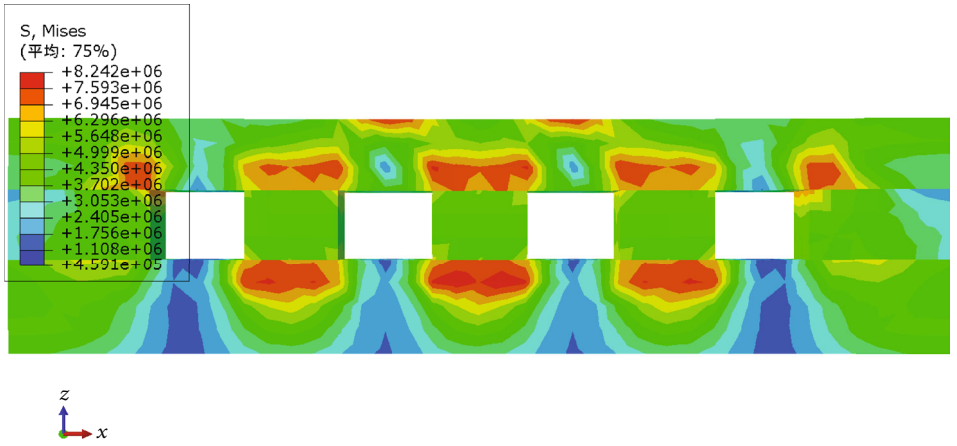

(a) 4 m

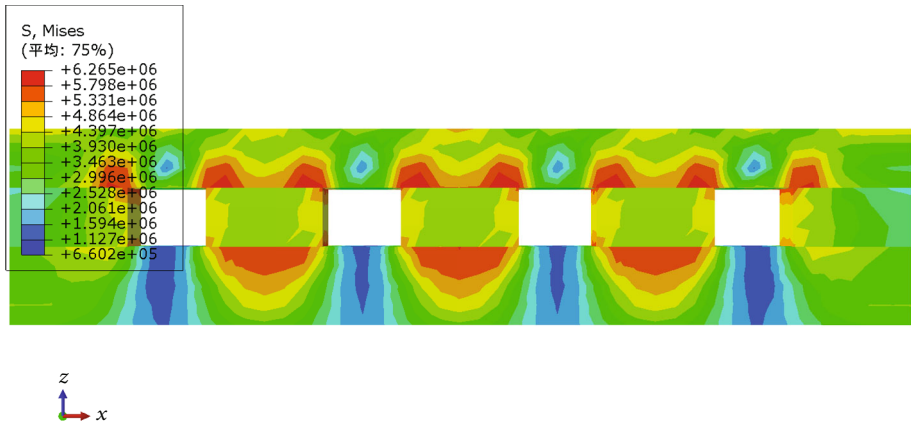

(b) 6 m

Figure 5: Stress distribution of the pillars with the width of 4 m and 6 m.

be 4 m and 6 m, respectively. The mechanical parameters of the pillar supporting system in the numerical model are shown in Table 1.

The numerical model included 9 pillars (3 × 3 layout). The model was 40 × 14 × 20 m. The size of the pillars was 4 × 4 × 4 m and 6 × 4 × 4 m, respectively. The size of the mine house was 4 × 4 × 4 m. The pillar model is shown in Figure 3. The upper, left, and right boundaries of the model were free. The cell grid type was C3D8I.

In the mine, the stability of the pillar supporting system was affected by various dynamic loads. The effects of the different disturbed stress on the stress, strain, and plastic zone of the pillar supporting system were studied. The load of 3.3 MPa was applied on the upper boundary of the numerical model. According to the uniaxial compressive strength of the pillar, the peak value of the stress wave was selected to be 6 MPa, 8 MPa, and 10 MPa, respectively. The disturbance time was 4 ms. The disturbance curve of the stress wave is shown in Figure 4.

3.2. Static Characteristic of Pillar Supporting System. The pillar supporting system was affected by both dynamic and static loads. Firstly, the initial geostress was applied as the prestress. Then, the pillar supporting system with a single pillar width of 4 m and 6 m was calculated, respectively. The stress distribution after in situ stress balance is shown in Figure 5.

It could be seen from Figure 5 that when the disturbed stress was 0, the stress concentration occurred at the roof and floor of the pillar due to the load of the overburden strata. The stress concentration of the roof-floor rock layers of the pillars with different widths was not alike. When the pillar width was 4 m, the maximum stress of the roof-floor rock layers was 8.242 MPa. The roof-floor rock layers had stress concentration directly above and below the pillars. And the stress distribution above the pillar was saddle shaped. The local stress concentration also appeared at the top of the model. The strata below the goaf had the lowest stress. When the pillar width was 6 m, the maximum stress of the roof-floor rock layers was 6.265 MPa. It can be seen from the comparison that as the pillar width increased, the maximum stress decreases, and then the risk of the pillar failure reduced. So, the 6 m wide pillar was more stable than the 4 m wide pillar.

4. Results and Analysis

After the stress waves were disturbed, the maximum stress, maximum principal strain, and PEEQ of the pillar supporting system were as follows.

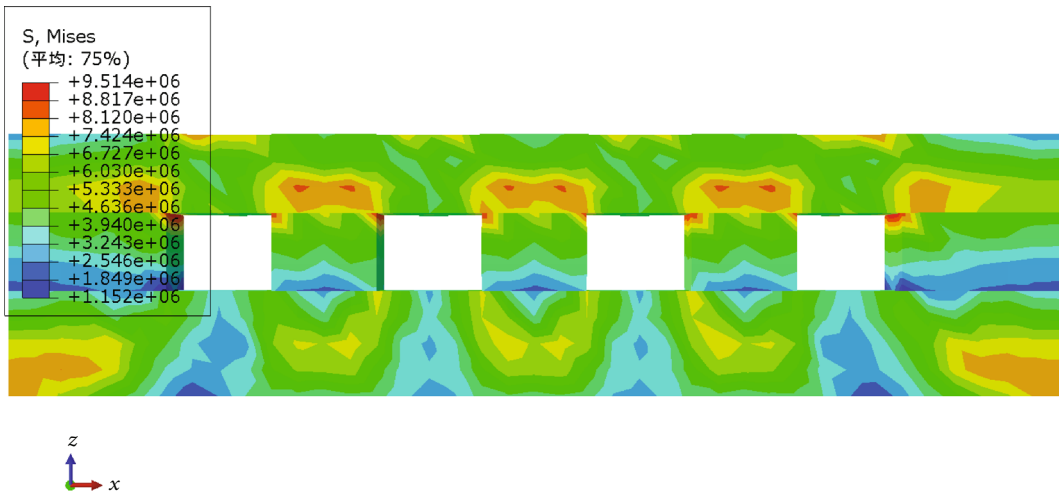

(a) 6 MPa

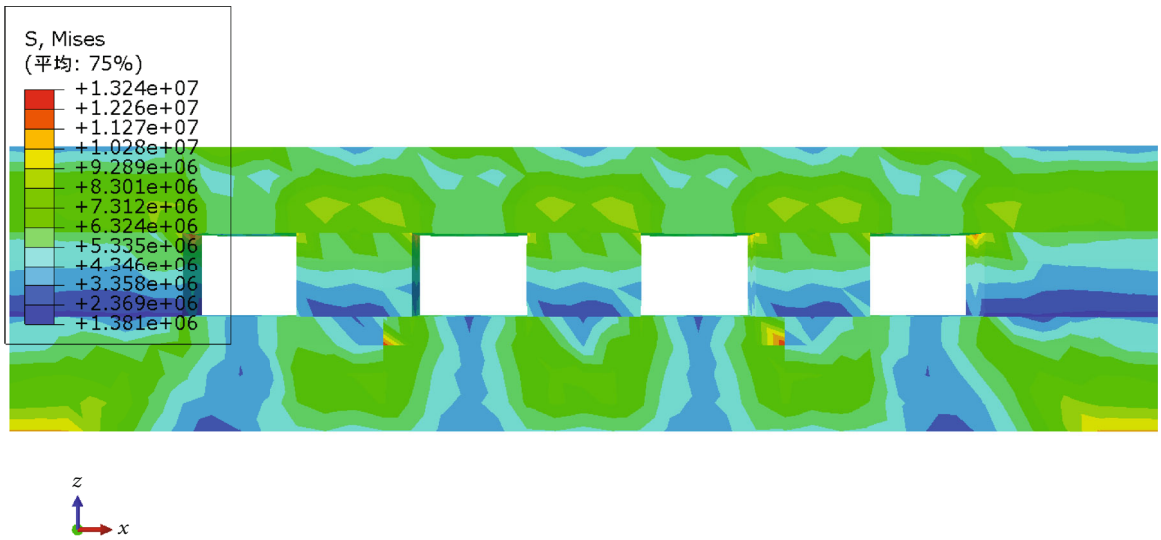

(b) 8 MPa

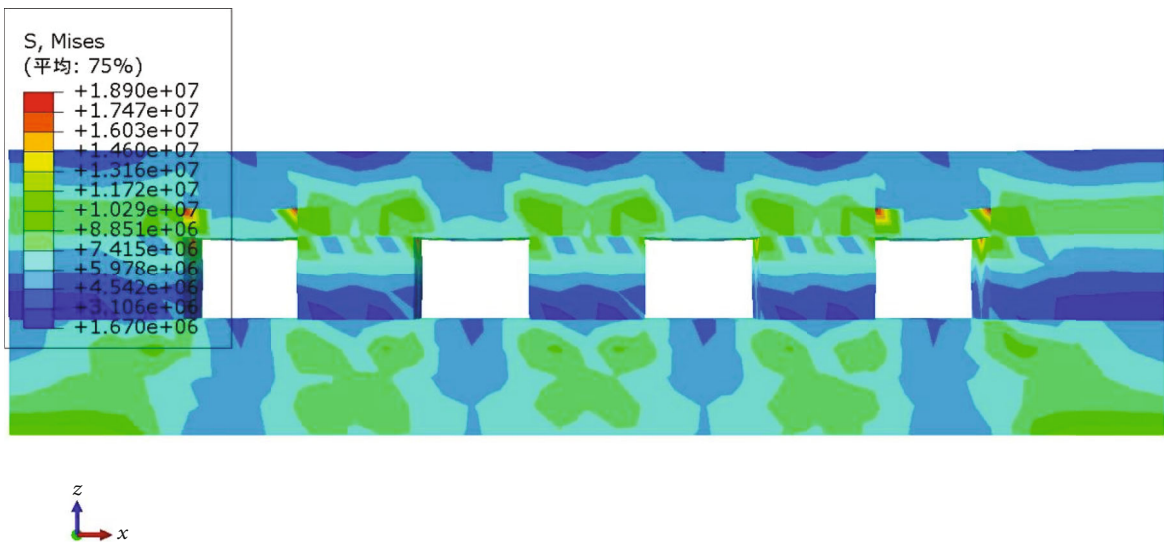

(c) 10 MPa

Figure 6: The stresses of the pillar supporting system with a single pillar width of 4 m.

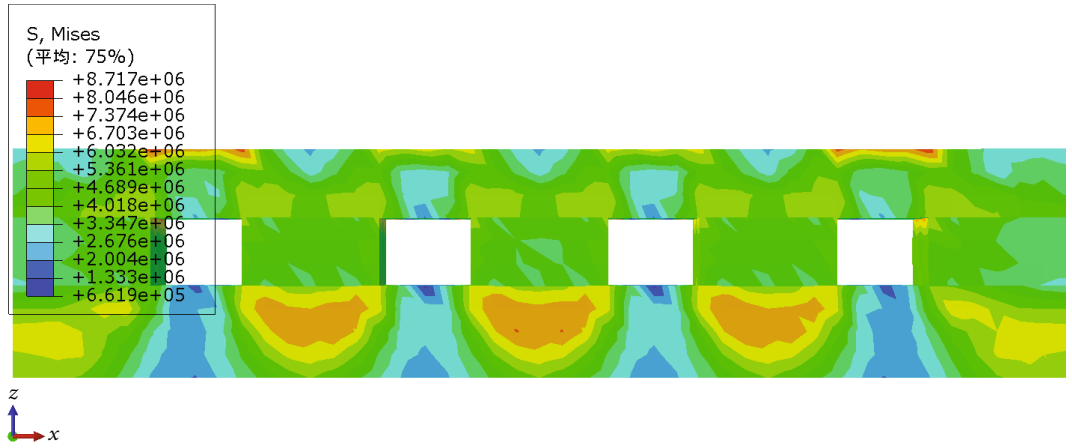

(a) 6 MPa

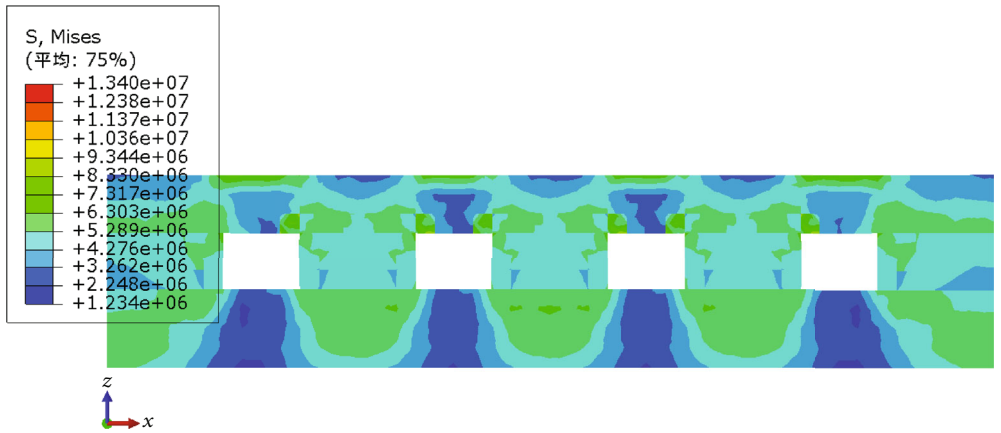

(b) 8 MPa

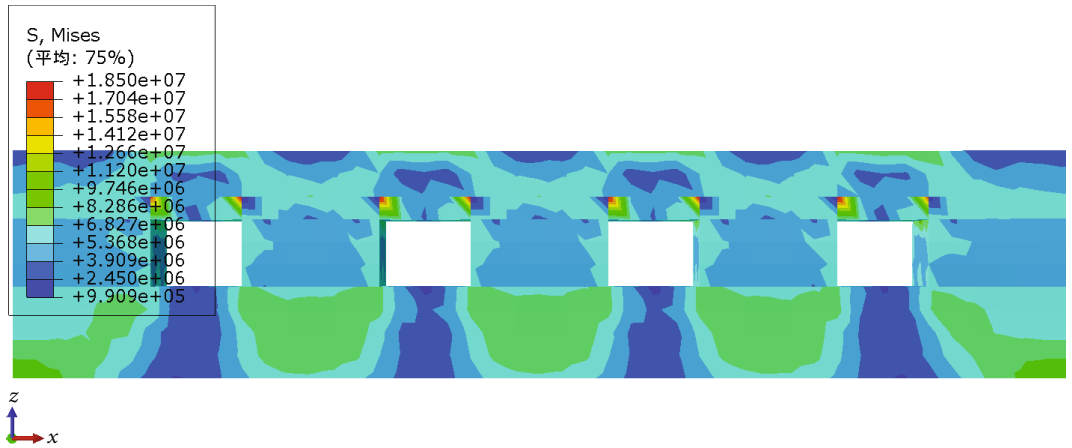

(c) 10 MPa

Figure 7: The stresses of the pillar supporting system with a single pillar width of 6 m.

4.1. Characteristics of Stress Distribution. After the stress waves of 6 MPa, 8 MPa, and 10 MPa were disturbed, the stresses of the pillar supporting system with a single pillar width of 4 m and 6 m are shown in Figures 6 and 7, respectively.

It could be seen that the internal stress of the pillar increased with the increase of the disturbed stress. It showed that the elastic energy inside the pillar increased with the increase of disturbed stress. The higher the peak value of the stress wave, the faster the elastic energy would increase. Under the same disturbed stress, with the increase of the pillar width, the stress of the pillar and its upper and lower rock layers was reduced. And the stress reduction of roof rock was the most obvious. It showed that 6 m wide pillars could withstand greater disturbed stress than 4 m wide pillars.

After the stress waves of 6 MPa, 8 MPa, and 10 MPa were disturbed, the maximum stresses of 4 m wide pillars were

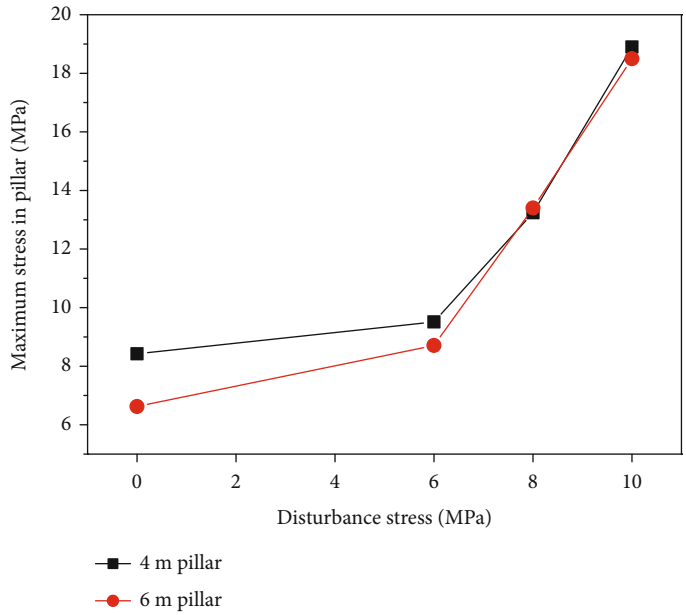

Figure 8: The growth curve of the maximum stress inside the pillar supporting system.

9.514 MPa, 13.24 MPa, and 18.90 MPa, respectively. Compared with the static maximum stress of 8.424 MPa, the maximum stress of 4 m wide pillar increased by 1.09 MPa, 4.818 MPa, and 10.478 MPa, respectively. With the larger disturbed stress, the faster the stress value of the 4 m wide pillar increased, the greater the elastic energy inside the pillar. When the peak value of disturbed stress increased by 2 MPa, the stress increments of 4 m wide pillars were 3.726 MPa and 5.66 MPa, respectively, with an average increase of 4.693 MPa, and the stress growth rates of the pillars were 39.16% and 42.74%, with an average growth rate of 40.95%.

After the stress waves of 6 MPa, 8 MPa, and 10 MPa were disturbed, the maximum stress values of 6 m wide pillars were 8.71MP, 13.4 MPa, and 18.50 MPa, respectively. Compared with the static maximum stress of 6.625 MPa, the maximum stress of 6 m wide pillar increased by 2.05 MPa, 6.775 MPa, and 11.875 MPa, respectively. With the larger disturbed stress, the faster the stress value of the 6 m wide pillar increases, the greater the elastic energy inside the pillar. When the peak value of disturbed stress increases by 2 MPa, the stress increments of 6 m wide pillars were 4.725 MPa and 5.1 MPa, respectively, with an average increase of 4.9125 MPa, and the stress growth rates of pillars were 54.24% and 38.06%, with an average growth rate of 46.15%.

The increase of the maximum stress of the pillar caused by the disturbed stress was nonlinear to the static stress. The greater the disturbed stress, the faster the stress increase rate of the pillar. The disturbed stress had the greatest influence on the central and upper apex angle of each pillar. When the peak value of the disturbed stress was 10 MPa, the stress concentration of the pillar also appeared in the grid position where the roof and the pillar were in contact, which may be caused by the stress concentration in the grid calculation.

Figure 8 showed the growth curve of the maximum stress inside the pillar supporting system. It could be seen that there was an approximately linear relationship between the maximum stress of the pillar and the peak value of the disturbed stress. So it was fitted by a linear formula. The fitting curves of the maximum stress value and disturbed stress inside the pillar supporting system with single pillar width of 4 m and 6 m were $y = 0.4086x + 2.4676$ and $y = 0.4204x + 2.1654$, respectively. With the increase of the disturbed stress, the maximum internal stress of the 6 m wide pillar increases faster. When the peak value of disturbed stress increases by 2 MPa, the average growth rate of the internal maximum stress value of 4 m and 6 m wide pillar was 40.95% and 46.15%.

Under the influence of less disturbed stress, the maximum stress of narrow pillar was greater than that of wide pillar. At this time, the local plastic deformation occurred in narrow pillars, but not in the wider pillar. As the disturbed stress increased, the plastic zone of the narrow pillar gradually expanded, while the wider pillar gradually changed from an elastic state to a local plastic state. The narrow pillar was destroyed first. The maximum stress of the narrow pillar was higher than that of the wide pillar.

4.2. Characteristics of Strain Distribution. After the stress waves of 6 MPa, 8 MPa, and 10 MPa were disturbed, the maximum principal strains of the pillar supporting system with single pillar width of 4 m and 6 m are shown in Figures 9 and 10, respectively.

It could be seen that the maximum principal strain of 4 m and 6 m wide pillars could be stable with the increase of the disturbed stress. But the maximum strain value of 4 m wide pillars was greater than that of 6 m wide pillars. The ability of 6 m wide pillars to resist damage was better than that of 4 m wide pillars. So, the stability of 6 m wide pillar was better. After the stress waves of 6 MPa, 8 MPa, and 10 MPa were disturbed, the maximum principal strains of 4 m wide pillar were 1.188×10^{-2}, 1.972×10^{-2}, and 4.652×10^{-2}, respectively. With the larger disturbed stress, the faster the maximum principal strain value of the 4 m wide pillar increased.

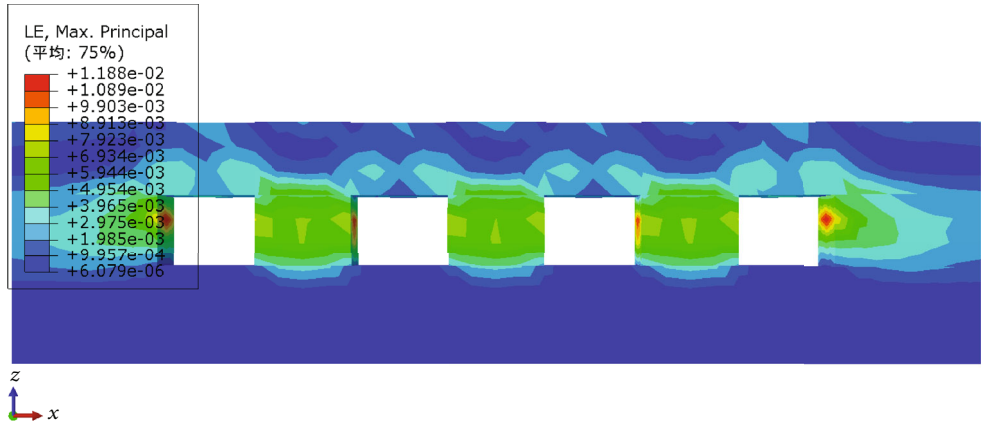

(a) 6 MPa

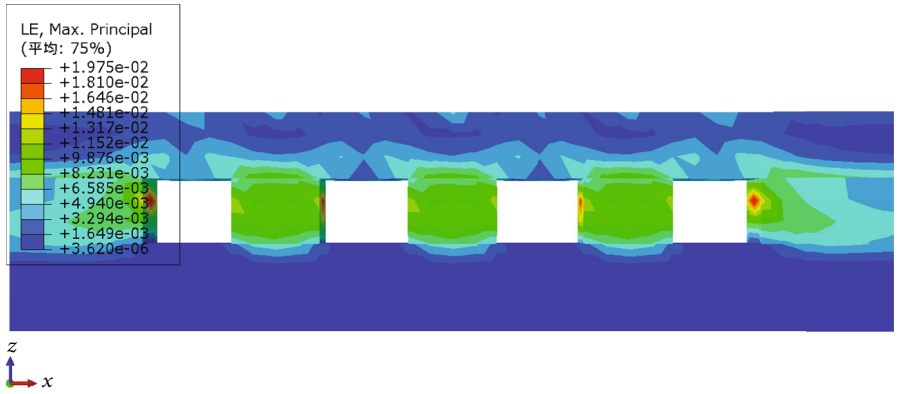

(b) 8 MPa

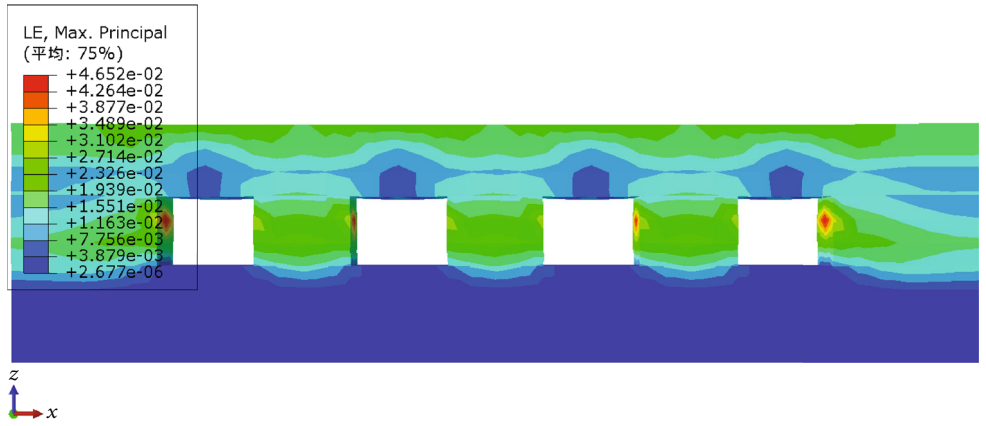

(c) 10 MPa

Figure 9: The maximum principal strain of the pillar supporting system with a single pillar width of 4 m.

When the peak value of disturbed stress increases by 2 MPa, the maximum principal strain increments of 4 m wide pillars were 0.784 and 2.68, respectively, and the growth rate of the maximum principal strain of the pillars were 65.9% and 135.9%. After the stress waves of 6 MPa, 8 MPa, and 10 MPa were disturbed, the maximum principal strains of 6 m wide pillars were 0.9803×10^{-2}, 1.749×10^{-2}, and 2.837×10^{-2}, respectively. When the peak value of disturbed stress increased by 2 MPa, the maximum principal strain increments of 6 m wide pillars were 0.766 and 1.088, respectively, and the growth rates of the maximum principal strain of pillars were 78.13% and 62.2%.

Figure 11 shows the growth curve of the maximum principal strain inside the pillar supporting system. It could be seen that there was an approximately linear relationship between the maximum principal strain of the 6 m wide pillars and the peak value of the disturbed stress. The growth rate of the maximum principal strain of the 4 m wide pillars was increasing. When the peak value of the disturbed stress was 10 MPa, the maximum main strain inside the 4 m wide

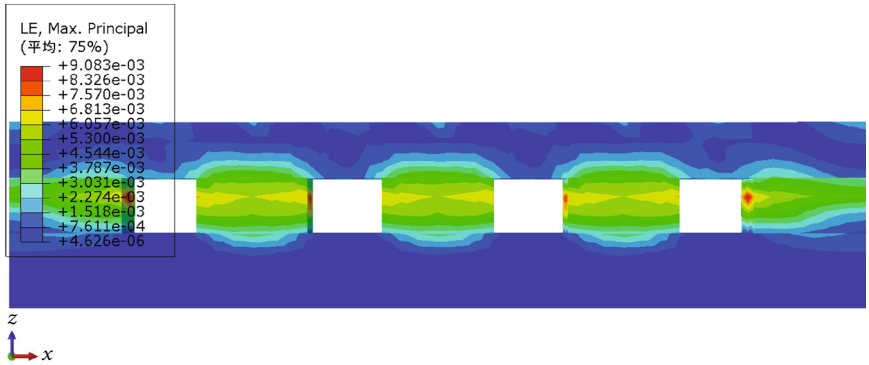

(a) 6 MPa

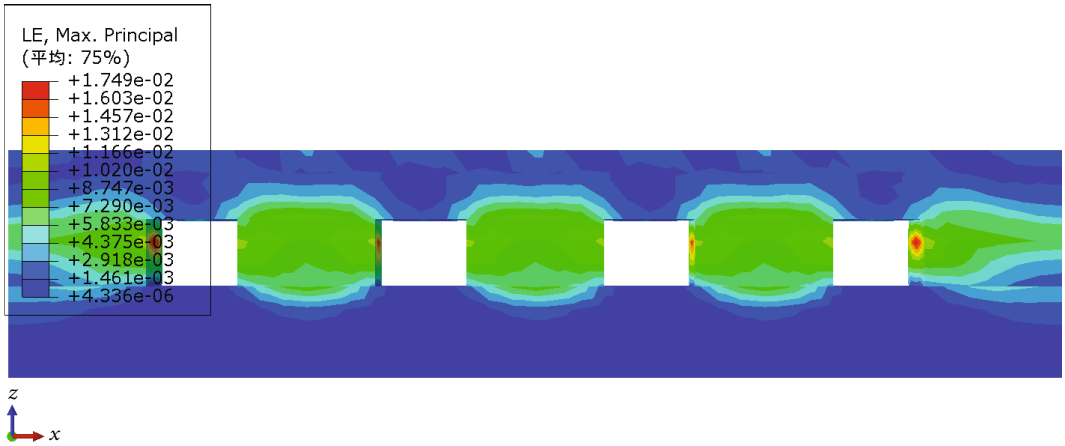

(b) 8 MPa

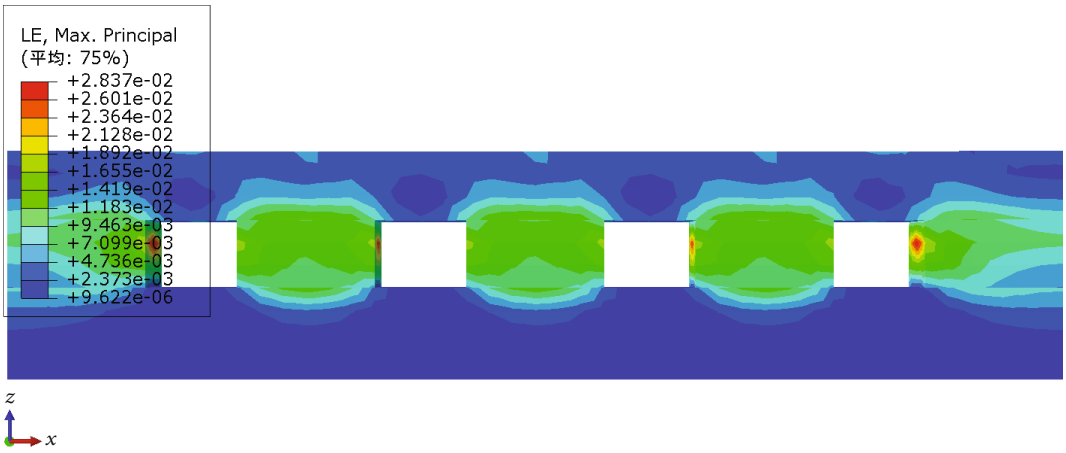

(c) 10 MPa

Figure 10: The maximum principal strain of the pillar supporting system with a single pillar width of 6 m.

pillar suddenly increased. It showed that under the disturbed stress of 10 MPa, the 4 m wide pillar may be damaged, and its growth value was exponential growth. However, the maximum principal strain of the 6 m wide pillar could still maintain stable growth. This showed that the 6 m wide pillars were more resistant to destruction. So, the load capacity of the pillar was limited. The greater the disturbed stress of the pillar, the greater the maximum principal strain growth rate.

The exponential fitting curves of the maximum principal strain value and disturbed stress inside the pillar supporting system with single pillar widths of 4 m and 6 m were $y = 0.1693e^{0.28x}$ and $y = 0.1447e^{0.34x}$. It could be seen that the maximum principal strain of 4 m wide pillar was 1.21 times that of 6 m wide pillar under the disturbed stress of 6 MPa. The maximum principal strain of 4 m wide pillar was 1.12 times that of 6 m wide pillar under the disturbed stress of 8 MPa. When the peak value of the disturbed stress was 10

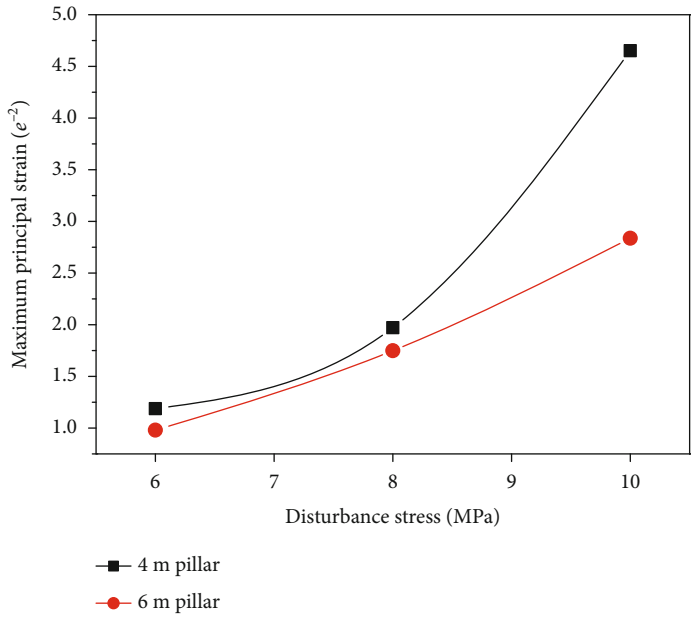

Figure 11: The growth curve of the maximum principal strain inside the pillar supporting system.

MPa, the maximum principal strain of 4 m wide pillar was 1.63 times that of 6 m wide pillar. Under three kinds of disturbed stresses, the maximum principal strain of 4 m wide pillars was 1.32 times that of 6 m wide pillars on average. So, under the disturbed stresses with different peaks, the ability of 6 m wide pillar to resist deformation was improved by 1.32 times than that of 4 m wide pillar.

4.3. PEEQ Analysis. After the disturbed stresses of 6 MPa, 8 MPa, and 10 MPa, the equivalent plastic strains of the pillar supporting system with single pillar width of 4 m and 6 m are shown in Figures 12 and 13, respectively.

With the increase of the disturbed stress, the disturbed range of the two pillars was enlarged. It could be seen from Figure 13 that the disturbed range of 6 m wide pillar was larger than that of 4 m wide pillar and the disturbed stress would aggravate the destruction of the pillar supporting system. Under the same disturbed stress, the support system of 6 m wide pillar was more resistant to damage than that of 4 m wide pillar. When the pillar was disturbed, the distributions of the equivalent plastic strain and the maximum principal strain were similar, both of which were distributed at the upper part of the pillar. After the stress waves of 6 MPa, 8 MPa, and 10 MPa were disturbed, the equivalent plastic strains of 4 m wide pillar were 6.395×10^{-2}, 1.082×10^{-1}, and 2.579×10^{-1}. When the peak value of disturbed stress increased by 2 MPa, the equivalent plastic strain increments of 4 m wide pillars were 0.4425 and 1.497, respectively, and the growth rates of the equivalent plastic strain of the 4 m wide pillars were 69.1% and 138.3%. After the stress waves of 6 MPa, 8 MPa, and 10 MPa were disturbed, the equivalent plastic strains of 6 m wide pillar were 4.653×10^{-2}, 8.49×10^{-2}, and 1.376×10^{-1}. When the peak value of disturbed stress increases by 2 MPa, the equivalent plastic strain increments of 6 m wide pillars were 0.384 and 0.527, respectively, and their growth rates were 82.46% and 62.07%.

Figure 14 shows the growth curve of the equivalent plastic strain inside the pillar supporting system. It could be seen that there was an approximately linear relationship between the equivalent plastic strain of the 6 m wide pillar and the disturbed stress. The growth rate of the equivalent plastic strain of the 4 m wide pillar was increasing. From the comparison between Figures 10 and 13, it could be seen that with the increase of the disturbed stress, the growth curves of the equivalent plastic strain of the pillar and the maximum principal strain were similar. Under the disturbed stress of 10 MPa, the equivalent plastic strain of the 4 m wide pillar suddenly increased. This indicated that the 4 m wide pillar might have been damaged, while the equivalent plastic strain of the 6 m wide pillar could still maintain a stable growth. The equivalent plastic strains of 4 m and 6 m wide pillars could be fitted with straight lines and exponential functions, respectively. The equivalent plastic strain formulas of the pillar supporting system with single pillar width of 4 m and 6 m were $y = 0.736e^{0.35x}$ and $y = 0.9332e^{0.27x}$, respectively. It could be seen that the equivalent plastic strain of 4 m wide pillar was 1.37 times that of 6 m wide pillar under the disturbed stress of 6 MPa. When the disturbed stresses were 8 MPa and 10 MPa, the equivalent plastic strain of 4 m wide pillar was 1.27 and 1.87 times that of 6 m wide pillar, respectively. Under three kinds of disturbed stresses, the equivalent plastic strain of 4 m wide pillars was 1.5 times that of 6 m wide pillars on average. After the peak value of disturbed stress was greater than 8 MPa, the plastic strain velocity of 4 m wide pillar was much larger than that of 6 m wide pillar. By comparing the relationship between different disturbed stresses, the maximum principal strain, and PEEQ growth, it could be seen that smaller disturbed stress would make the internal elastic energy of the pillar larger and larger, while larger disturbed stress would increase the damage degree and rate of the pillar.

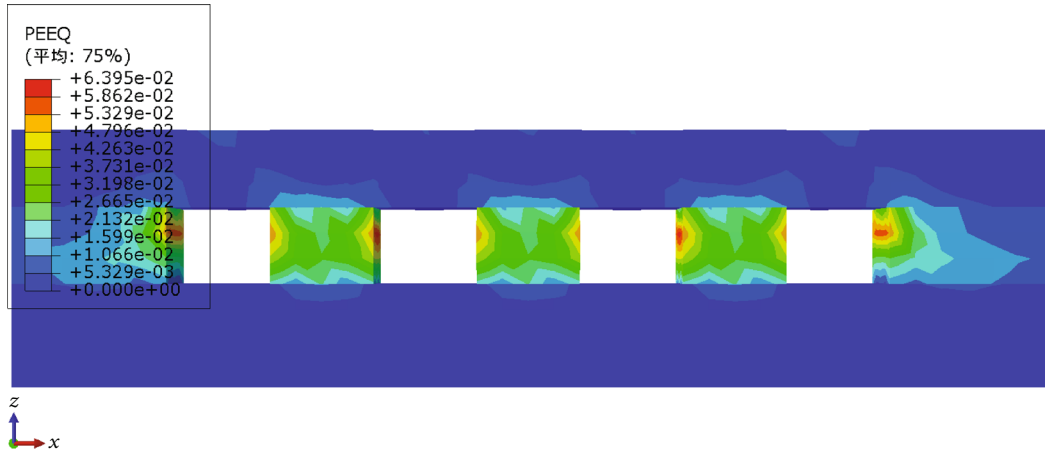

(a) 6 MPa

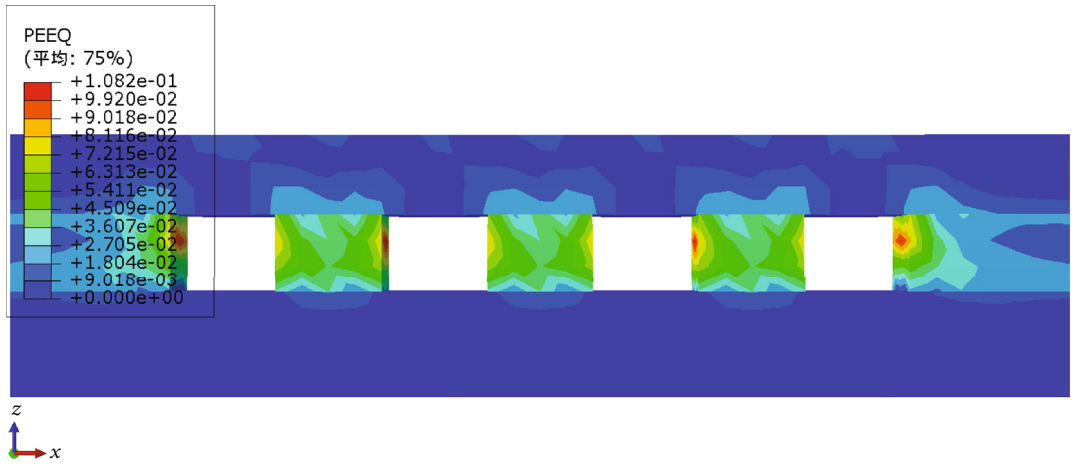

(b) 8 MPa

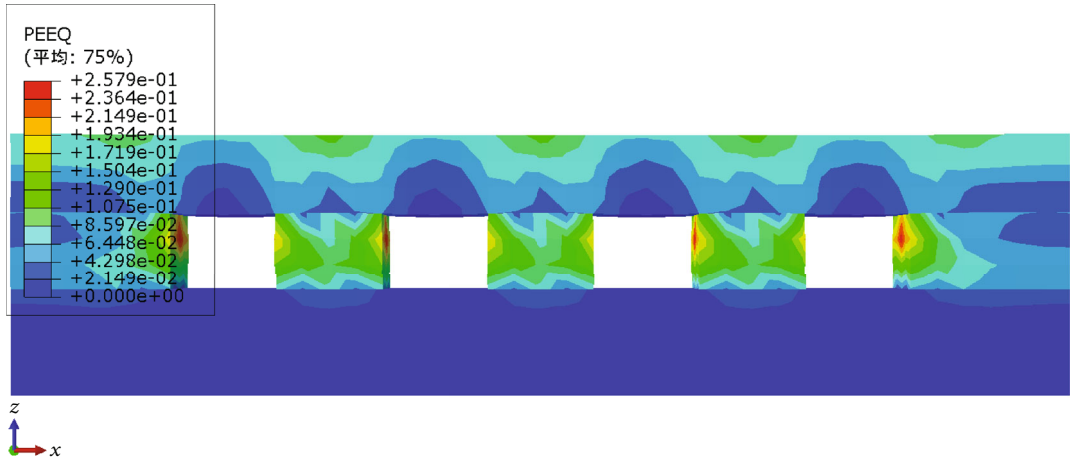

(c) 10 MPa

Figure 12: The equivalent plastic strain of the pillar supporting system with a single pillar width of 4 m.

5. Domino Instability Effect of Pillar Supporting System

The cascading chain reaction caused by a small change, resulting in a huge range of effects, was called the domino effect. In the process of mining, it was usually the single pillar under the influence of multiple factors that was destroyed. This causes the stress to retransfer, which in turn leads to an increase in the stresses of multiple pillars. In an appropriate space and time, the overall failure of the multiple pillars will occur, which in turn triggers the domino instability effect of the pillar supporting system. It might cause serious disasters.

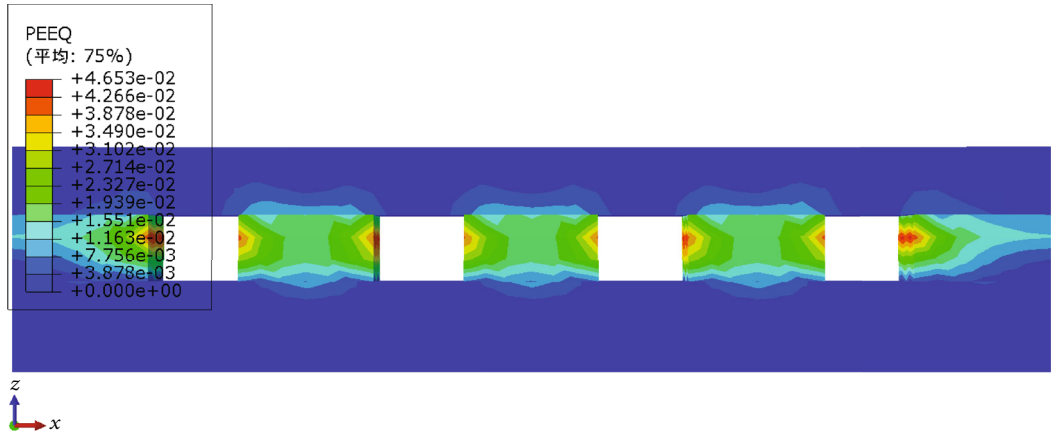

(a) 6 MPa

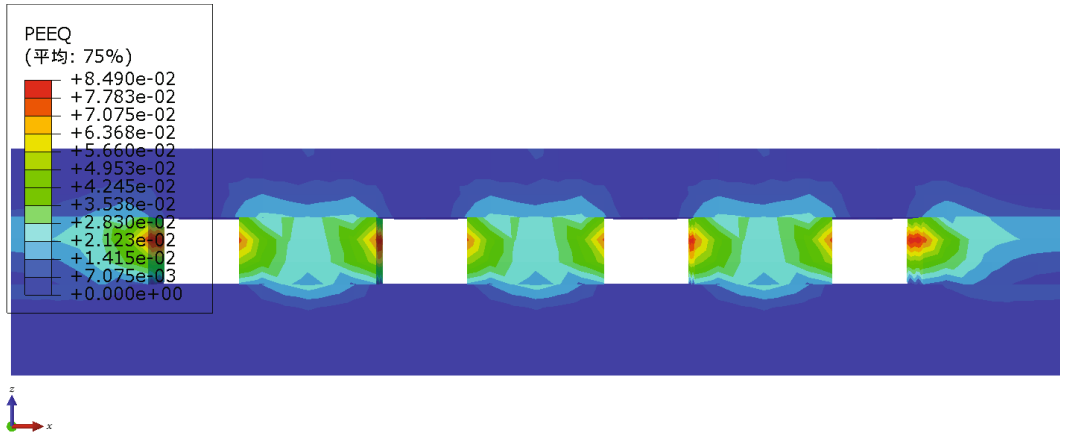

(b) 8 MPa

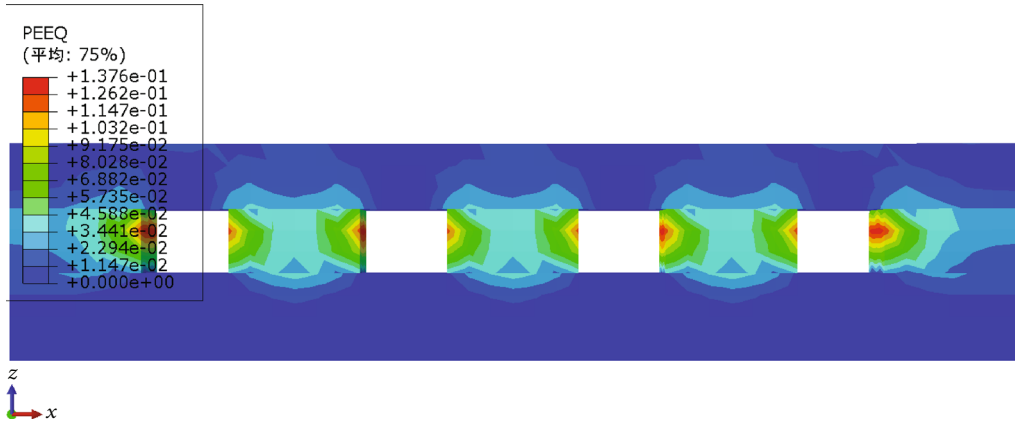

(c) 10 MPa

Figure 13: The equivalent plastic strain of the pillar supporting system with a single pillar width of 6 m.

It could be seen from the change law of stress, strain, and plastic zone of the pillar supporting system under the disturbed stress that the central part of the pillar was damaged most seriously. The compression failure of a single pillar occurs first in its upper part, thereby increasing its internal stress, which in turn causes the overall instability. The following was the numerical simulation to investigate the domino instability law of the pillar supporting system caused by the destruction of a single pillar.

Figure 15 shows the stress distribution of the pillar before and after instability. After reducing the width of the middle pillar by 0.5 m, respectively, the results showed that the stress concentration area of the overlying strata of the middle pillar increased significantly. The maximum internal stress of the pillar was 12.95 MPa, which was 57.12% higher than that of the 4 m wide pillar. After the width of the middle pillar became 3.5 m, the pillar supporting system was destroyed.

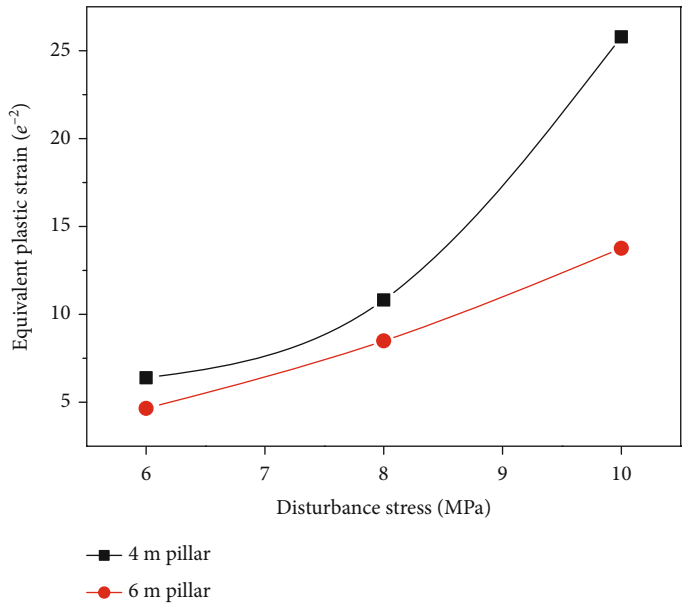

Figure 14: The growth curve of the equivalent plastic strain inside the pillar supporting system.

It could be seen from Figure 15(b) that the instability of the middle pillar caused the stress of the overlying strata to be transmitted to both sides, and the stress of the adjacent pillars also increased significantly. The stress at the bottom of the pillars was the largest. The maximum principal stress of the pillar supporting system reached 21.20 MPa, an increase of 63.71% compared with before the failure. During the destruction of the pillar, the stress of the pillar would increase exponentially. So, the stress monitoring meter was arranged to survey the internal stress of the pillar supporting system to prevent the overall failure.

During the destruction process of the pillar, its plastic zone continued to expand. Figure 16 shows the destruction process of the pillar supporting system. The equivalent plastic strain of the system was 4.622. Firstly, the middle pillar was destroyed. With the increase of the stress, the plastic area inside the middle pillar was enlarged and gradually penetrated, causing it to be destroyed first. The load of the overlying strata was transmitted to the adjacent pillar, which in turn causes its stress to increase. The plastic zone of the adjacent pillar first appeared on the edge of the middle pillar. The load transmission of the overlying strata was symmetrical to both sides, so the plastic zone of the pillar supporting system was symmetrically distributed. As the load gradually shifted to both sides, the plastic zone of adjacent pillars gradually penetrated. Furthermore, the adjacent pillars were destroyed. The support system of the pillar had suffered from overall instability.

It could be seen from the above analysis that the failure of a single pillar may cause the instability of the adjacent pillars, which in turn might result in the chain instability of pillar supporting system. In the process of room-pillar mining, the external disturbance had exacerbated the chain destruction degree of the pillar supporting system. This was because external disturbances provided dynamic waves, which made the pillars in equilibrium unable to bear the combined effects of dynamic and static loads. For the mined-out area of room-pillar mining, the destruction of a single pillar might cause explosive destabilization of the surrounding pillars. It caused large-scale collapse of the roof strata in the mined-out area, which in turn may cause surface subsidence and environmental damage.

6. Case Analysis and Monitoring Methods

It could be seen from the above analysis that the disturbed stress with different peaks had increased the plastic zone of the pillar, which in turn reduces its bearing capacity. There were not many examples of the overlying strata instability caused by the destruction of a single pillar. So, it is necessary to prevent the overall instability of the pillars.

6.1. Case Analysis. The instability of local mined-out areas often caused the surface to sink slowly. When the large-scale pillars were unstable, the instantaneous instability of the overlying strata and the sudden collapse of the surface often occurred. On June 9, 1986, the 800 m^2 roof of Beicun Coal Mine in Datong, China, collapsed. Then, the nearby Xiaonantou Mine, Jiucaigou Mine, and 51056 Troop Mine successively suffered large-scale roof rock collapsed. The total collapse area reached 89,425 m^2. On June 13, a sudden subsidence occurred on the ground, covering an area of 80,500 m^2, which caused significant economic losses [35]. This accident was a typical domino effect caused by the local destruction of the pillars, which caused the overall instability of the pillar supporting system.

The local pillar instability in the Beicun Coal Mine caused the gravity stress of the rock layer to shift to the adjacent

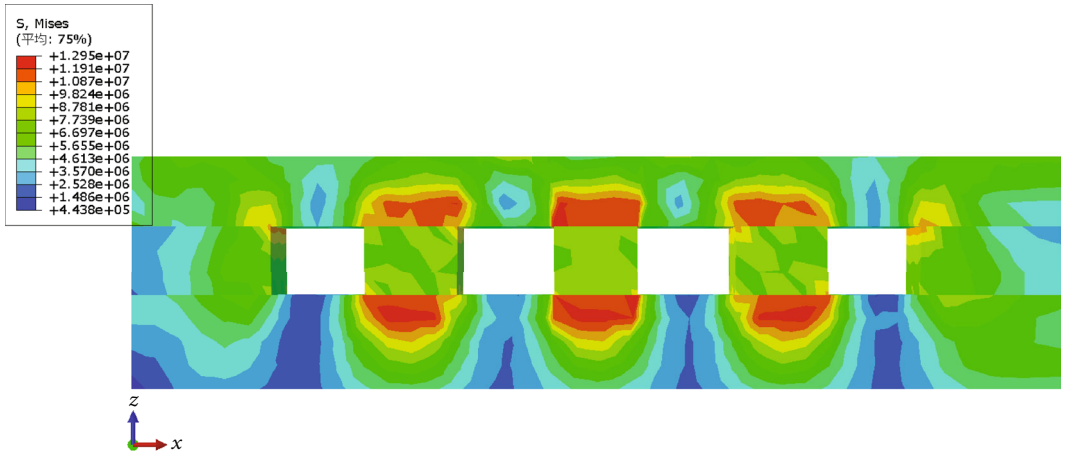

(a) Before instability

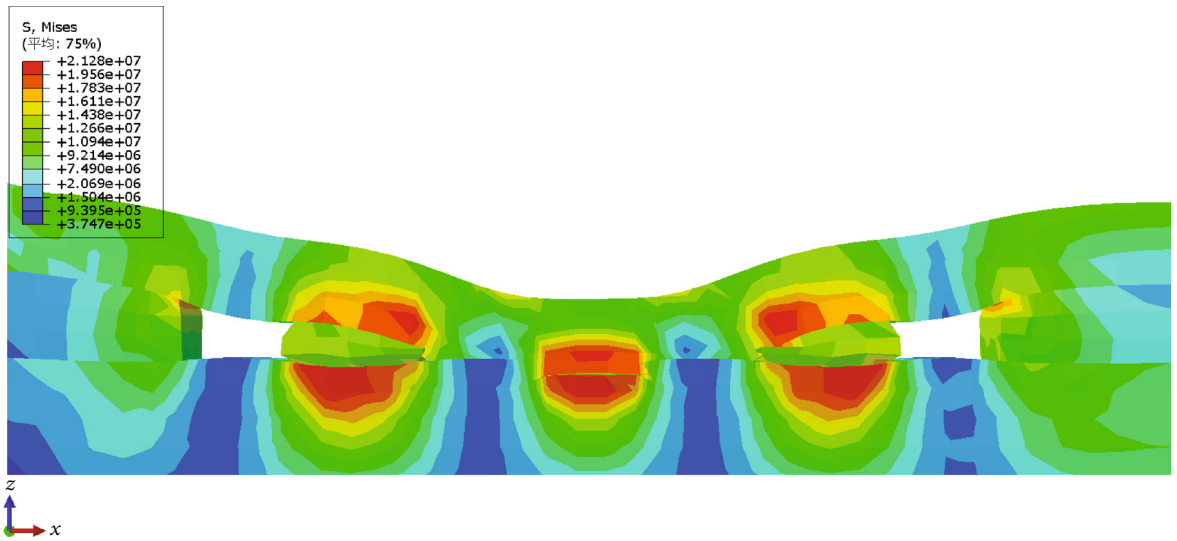

(b) After instability

Figure 15: The stress distribution of the pillar before and after instability.

pillars, gradually leading to the large-scale pillar instability. However, the large-scale movement of the roof strata caused the gravity stress of the strata to be transferred to the adjacent mines, which also resulted in the instability of the adjacent goaf. During mining, the blasting will generate a lot of disturbed stress. The disturbed stress with a lower peak value would cause the elastic energy in the pillar to increase. The disturbed stress with a larger peak value would aggravate the damage degree of the pillar.

According to the rescued workers, there was no obvious abnormality in the pillars and roof strata before the overall instability occurred. When the overall instability occurred, the vibration can be felt on the ground. A yellow column erupted from the relevant wellbore, and a roar similar to the takeoff of the aircraft was heard. After that, the cracks and collapses appeared on the surface. There was a lot of damage to surface buildings.

6.2. Monitoring Methods. According to the simulation results, when the pillar was destabilized, its maximum stress, maximum principal strain, and equivalent plastic strain all had a leaping-up phase. It could be monitored and forecasted by the underground monitoring device to prevent the instability of a single pillar from causing the overall instability of the goaf.

Commonly used equipment for stress monitoring includes borehole stress tester, stress pillows, and anchor ergometer. The stability of the pillar supporting system can be judged according to its stress growth trend. Commonly used strain monitoring equipment usually includes convergence gauge, multipoint extensometer, and sliding extensometer. The monitoring strain inside the pillar can provide the most direct judgment standard for the instability of a single pillar. In addition, by monitoring the stress wave and electromagnetic radiation signal of the pillar, the possibility of rock destruction and instability disasters can be predicted.

According to the simulation results, the instability of the pillar supporting system will first start from the central pillar. So, the central pillar should be the key monitoring object. By

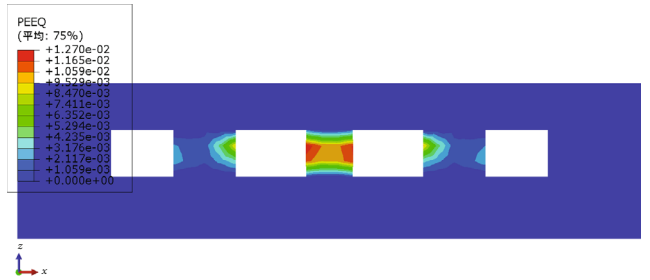

(a)

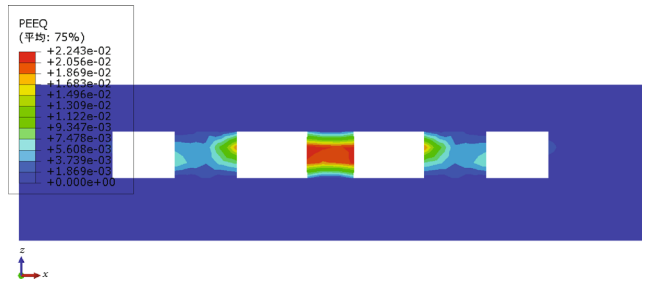

(b)

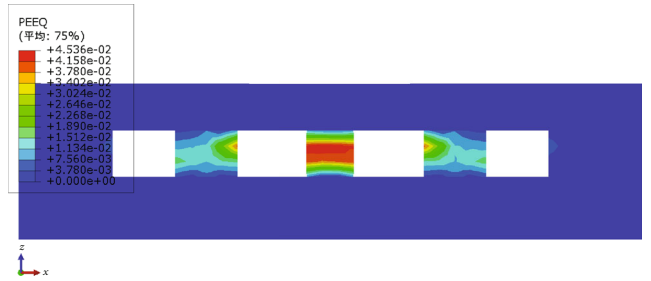

(c)

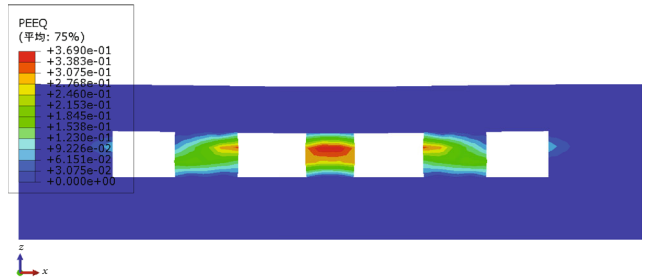

(d)

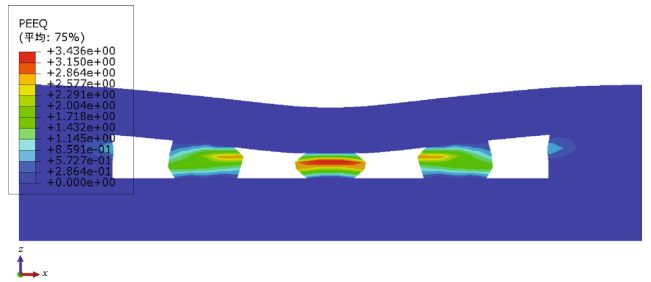

(e)

Figure 16: Continued.

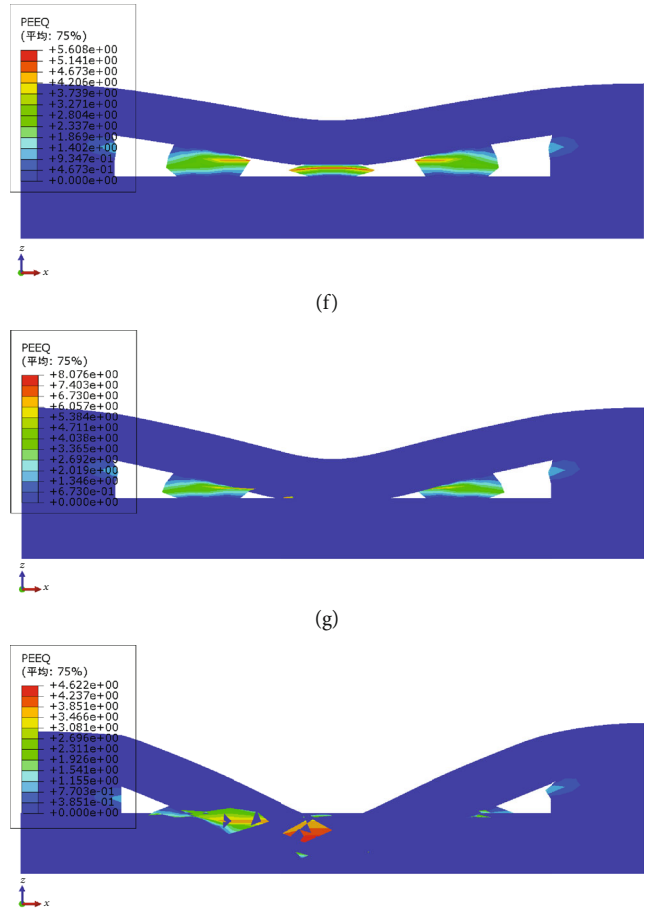

Figure 16: The destruction process of the pillar supporting system.

arranging stress monitoring points, displacement monitoring points, or plastic strain monitoring points in the central pillar and the roof-floor rock layers, the stability of the pillar can be evaluated by analyzing the data recorded continuously for a period of time.

7. Discussion

Zhou et al. [36] showed that after the weaker pillar failed, the stress of the adjacent pillars and its roof-floor rock layers would be redistributed. When the load of the roof rock layer on the pillars is close to their bearing capacity, the instability of a single pillar will inevitably cause the overall instability of the pillar supporting system. In this period, the average stress of the system remains almost unchanged. When the bearing capacity of the pillars is much greater than the load of the roof rock layer, the instability of a single pillar will not cause a chain instability of the pillar supporting system. So, it is the premise of the whole system instability that the load of the pillars is close to their bearing capacity.

Based on this, the instability of a single pillar will cause the redistribution of stress in the overlying strata, making the acting load of the stratum easily exceed the bearing capacity of the pillars. In addition, under the external disturbed stress, the stress balance state of the pillar supporting system may be broken. The external disturbed stress first breaks the stable state of the weakest pillars, which in turn leads to a chain instability of the pillar supporting system. So, the external disturbed stress is the fuse of chain instability of the pillar supporting system.

The middle pillars in the system were selected to analyze the distribution of stress and strain at different locations. Because the response of 4 m wide pillar to disturbed stress was more obvious than that of 6 m wide pillar, the left-section and midsection of 4 m middle pillar were selected for analysis. Under the disturbed stresses of 6 MPa, 8 MPa, and 10 MPa, the maximum stress and maximum principal strain of the left-section and midsection of the middle pillar are shown in Figure 17. Under each disturbed stress, the stress and strain at the edge of the middle pillar were larger than that at the middle. It showed that the stress distribution of the middle pillar was uneven. A certain degree of stress concentration appeared at the edge of the middle pillar. So, the edge of the middle pillar was plastically destroyed first and then gradually penetrated the entire pillar, causing instability.

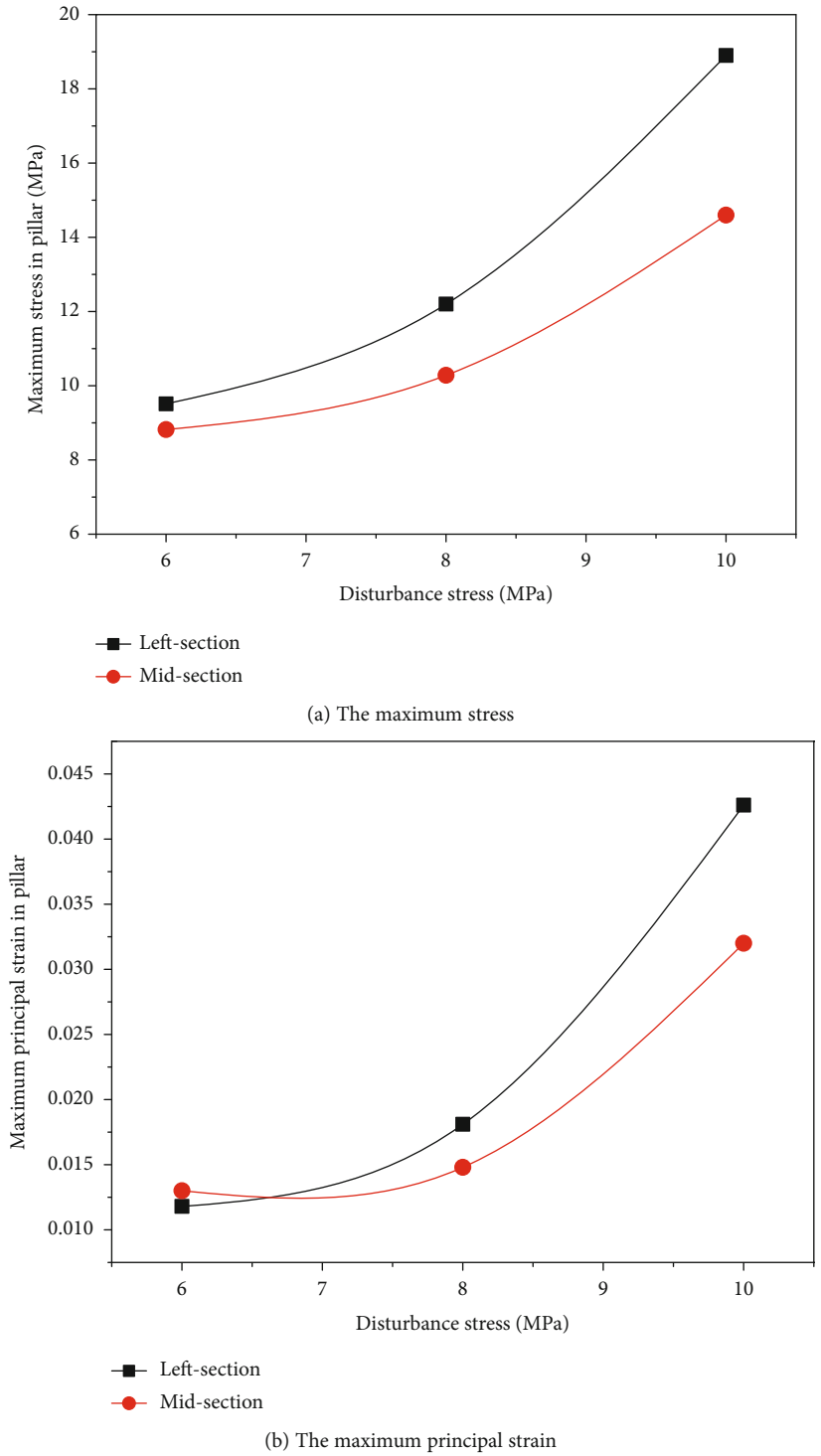

Figure 17: The maximum stress and the maximum principal strain of the middle pillar under different disturbed stresses.

8. Conclusion

(1) The strain and stress of the pillar are closely related to the disturbed stress. Without any disturbed stress conditions, the stress concentration occurs at the roof and floor of the pillar. The maximum stress values of the 4 m and 6 m wide pillars were 8.242 MPa and 6.265 MPa, respectively. As the pillar width increased, its maximum stress decreased, so its risk of failure reduced

(2) The disturbed stress was nonlinear with the increase of the maximum stress of the pillar supporting system. The greater the peak value of the disturbed stress, the faster the increase rate of the internal stress of the pillar, which was more destructive to the pillar.

As the width of the pillar increased, the stress of the pillar and roof-floor rock layers decreased, especially for the roof rock layer

(3) With the increase of the disturbed stress, the maximum principal strain and equivalent plastic strain of the 6 m wide pillar increased approximately linearly, and the growth rate of the maximum principal strain and equivalent plastic strain of the 4 m wide pillar gradually increased. Under the three disturbed stresses, the maximum principal strain and equivalent plastic strain of the 4 m wide pillar were 1.32 times and 1.5 times that of the 6 m wide pillar, respectively

(4) In the process of chain instability of the pillar supporting system, the sides of the middle pillar were destroyed first. The self-weight stress of the overlying rock layer was transmitted to the surroundings, which caused the destruction of the adjacent pillars. The external disturbed stress aggravated the degree of chain instability of the pillar supporting system. By arranging stress monitoring points, displacement monitoring points, or plastic strain monitoring points in the central pillar and the roof-floor rock layers, the stability of the pillar can be evaluated by analyzing the data recorded continuously for a period of time

Data Availability

The data comes from numerical simulation results. Numerical simulation cloud images have been shown in the article. I promise that the data used is true and reliable without any modification.

Conflicts of Interest

The authors declare that there are no conflicts of interest.

Acknowledgments

This study was supported by Shandong Province Key R&D Plan (2018GSF116006).

References

[1] B. Li, R. Bao, Y. Wang, R. Liu, and C. Zhao, "Permeability evolution of two-dimensional fracture networks during shear under constant normal stiffness boundary conditions," *Rock Mechanics and Rock Engineering*, vol. 54, no. 1, pp. 409–428, 2021.

[2] A. Li, F. Dai, Y. Liu, H. B. Du, and R. C. Jiang, "Dynamic stability evaluation of underground cavern sidewalls against flexural toppling considering excavation-induced damage," *Tunnelling and Underground Space Technology*, vol. 112, 2021.

[3] Q. X. Meng, W. Y. Xu, H. L. Wang, X. Y. Zhuang, W. C. Xie, and T. Rabczuk, "DigiSim-an open source software package for heterogeneous material modeling based on digital image processing," *Advances in Engineering Software*, vol. 148, p. 102836, 2020.

[4] Q. Wang, H. K. Gao, B. Jiang, S. C. Li, M. C. He, and Q. Qin, "In-situ test and bolt-grouting design evaluation method of underground engineering based on digital drilling," *International Journal of Rock Mechanics and Mining Sciences*, vol. 138, 2021.

[5] Q. Wang, Q. Qin, B. Jiang et al., "Mechanized construction of fabricated arches for large-diameter tunnels," *Automation in Construction*, vol. 124, p. 103583, 2021.

[6] Y. Wang, W. K. Feng, R. L. Hu, and C. H. Li, "Fracture evolution and energy characteristics during marble failure under triaxial fatigue cyclic and confining pressure unloading (FC-CPU) conditions," *Rock Mechanics and Rock Engineering*, vol. 54, no. 2, pp. 799–818, 2021.

[7] Q. H. Gu, J. G. Ning, Y. L. Tan, X. S. Liu, Q. Ma, and Q. Xu, "Damage constitutive model of brittle rock considering the compaction of crack," *Geomechanics and Engineering*, vol. 15, no. 5, pp. 1081–1089, 2018.

[8] Q. Wang, B. Jiang, L. Wang et al., "Control mechanism of roof fracture in no-pillar roadways automatically formed by roof cutting and pressure releasing," *Arabian Journal of Geosciences*, vol. 13, no. 6, p. 274, 2020.

[9] Q. Wang, S. Gao, B. Jiang et al., "Rock-cutting mechanics model and its application based on slip-line theory," *International Journal of Geomechanics*, vol. 18, no. 5, article 04018025, 2018.

[10] Z. Xie, N. Zhang, X. Feng, D. Liang, Q. Wei, and M. Weng, "Investigation on the evolution and control of surrounding rock fracture under different supporting conditions in deep roadway during excavation period," *International Journal of Rock Mechanics and Mining Sciences*, vol. 123, 2019.

[11] D. W. Yin, S. J. Chen, B. Li, and W. J. Guo, "Bed separation backfill to reduce surface cracking due to mining under thick and hard conglomerate: a case study," *Royal Society Open Science*, vol. 6, no. 8, p. 190880, 2019.

[12] D. W. Yin, S. J. Chen, B. Chen, and Z. G. Xia, "Simulation study on strength and failure characteristics of coal-rock composite sample coal persistent joint," *Archives of Mining Sciences*, vol. 64, no. 3, pp. 609–623, 2019.

[13] A. Zingano and A. Weiss, "Subsidence over room and pillar retreat mining in a low coal seam," *International Journal of Mining Science and Technology*, vol. 29, no. 1, pp. 51–57, 2019.

[14] W. J. Yu and W. J. Wang, "Strata movement induced by coal-pillar under three circumstances exchanged by gangue backfill and quadratic stability law," *Chinese Journal of Rock Mechanics and Engineering*, vol. 30, no. 1, pp. 105–112, 2011.

[15] J. T. Li and P. Cao, "Cusp catastrophe model of instability of pillar in asymmetric mining," *Applied Mathematics and Mechanics*, vol. 26, no. 8, pp. 1100–1106, 2005.

[16] Y. L. Zhao, Q. Y. Peng, W. Wan, W. J. Wang, and B. Chen, "Fluid–solid coupling analysis of rock pillar stability for concealed karst cave ahead of a roadway based on catastrophic theory," *International Journal of Mining Science and Technology*, vol. 24, no. 6, pp. 737–745, 2014.

[17] C. Xiao, H. C. Zheng, X. L. Hou, and X. J. Zhang, "A stability study of goaf based on mechanical properties degradation of rock caused by rheological and disturbing loads," *International Journal of Mining Science and Technology.*, vol. 25, no. 5, pp. 741–747, 2015.

[18] X. B. Xie, R. N. Deng, X. J. Dong, and Z. Z. Yan, "Stability of goaf group system based on catastrophe theory and rheological theory," *Rock and Soil Mechanics*, vol. 39, no. 6, pp. 1963–1972, 2018.

[19] E. Pourjavad and R. V. Mayorga, "A fuzzy rule-based approach to prioritize third-party reverse logistics based on sustainable development pillars," *Journal of Intelligent and Fuzzy Systems*, vol. 35, no. 3, pp. 3125–3138, 2018.

[20] X. Y. Wang, J. B. Bai, R. F. Wang, and W. L. Sheng, "Bearing characteristics of coal pillars based on modified limit equilibrium theory," *International Journal of Mining Science and Technology*, vol. 25, no. 6, pp. 943–947, 2015.

[21] W. Y. Guo, Q. H. Gu, Y. L. Tan, and S. C. Hu, "Case studies of rock bursts in tectonic areas with facies change," *Energies*, vol. 12, no. 7, 2019.

[22] R. Singh, A. K. Singh, J. Maiti, P. K. Mandal, R. Singh, and R. Kumar, "An observational approach for assessment of dynamic loading during underground coal pillar extraction," *International Journal of Rock Mechanics and Mining Sciences*, vol. 48, no. 5, pp. 794–804, 2011.

[23] S. L. Wang, S. P. Hao, Y. Chen, J. B. Bai, X. Y. Wang, and Y. Xu, "Numerical investigation of coal pillar failure under simultaneous static and dynamic loading," *International Journal of Rock Mechanics and Mining Sciences*, vol. 84, pp. 59–68, 2016.

[24] W. J. Guo, H. L. Wang, and S. J. Chen, "Coal pillar safety and surface deformation characteristics of wide strip pillar mining in deep mine," *Arabian Journal of Geosciences*, vol. 9, no. 2, 2016.

[25] R. Gao, B. Yu, and X. B. Meng, "Stress distribution and surrounding rock control of mining near to the overlying coal pillar in the working face," *International Journal of Mining Science and Technology*, vol. 29, no. 6, pp. 881–887, 2019.

[26] J. G. Kim, W. R. Abdellah, and H. S. Yang, "Parametric stability analysis of pillar performance at Nohyun limestone mine, South Korea-a case study," *Arabian Journal of Geoscience*, vol. 12, no. 12, 2019.

[27] L. Xue-Hua, L. Wei-Dong, W. Yi-Pin, and Z. Shou-Song, "Analysis of bearing mechanism and influencing factors about dual structure of pillar and filling," *Procedia Earth and Planetary Science*, vol. 1, no. 1, pp. 294–302, 2009.

[28] P. Zhang, H. Dougherty, D. Su, J. Trackemas, and B. Tulu, "Influence of longwall mining on the stability of gas wells in chain pillars," *International Journal of Mining Science and Technology*, vol. 30, no. 1, pp. 3–9, 2020.

[29] E. Ghasemi, M. Ataei, and K. Shahriar, "An intelligent approach to predict pillar sizing in designing room and pillar coal mines," *International Journal of Rock Mechanics and Mining Sciences*, vol. 65, pp. 86–95, 2014.

[30] E. J. Cording, Y. M. A. Hashash, and J. Oh, "Analysis of pillar stability of mined gas storage caverns in shale formations," *Engineering Geology*, vol. 184, pp. 71–80, 2015.

[31] H. Wagner, T. Ladinig, and H. Blaha, "Design considerations for pillar systems in deep mines," *Geomechanics and Tunnelling*, vol. 9, no. 5, pp. 524–528, 2016.

[32] B. Yu, Z. Y. Zhang, T. J. Kuang, and J. R. Liu, "Stress changes and deformation monitoring of longwall coal pillars located in weak ground," *Rock Mechanics and Rock Engineering*, vol. 49, no. 8, pp. 3293–3305, 2016.

[33] S. J. Chen, D. W. Yin, H. M. Liu, B. Chen, and N. Jiang, "Effects of coal's initial macro-cracks on rockburst tendency of rock-coal composite samples," *Royal Society open science*, vol. 6, no. 11, p. 181795, 2019.

[34] X. B. Li, D. Y. Li, L. Guo, and Z. Y. Ye, "Study on mechanical response of highly-stressed pillars in deep mining under dynamic disturbance," *Chinese Journal of Rock Mechanics and Engineering*, vol. 2, no. 5, pp. 922–928, 2007.

[35] H. T. Ma, *Study on Method of Risk Classification and Instability Forecasting of Goaf*, University of science and technology Beijing, Beijing, China, 2015.

[36] Z. L. Zhou, L. Chen, X. Cai, B. T. Shen, J. Zhou, and K. Du, "Experimental investigation of the progressive failure of multiple pillar-roof system," *Rock Mechanics and Rock Engineering*, vol. 51, no. 5, pp. 1629–1636, 2018.